LA-UR -88-1476

CONF-880646--3

JUN 0 3 1988

TITLE: "Performance of the Los Alamos Expanding Telescope"

LA-UR--88-1476

DE88 010924

AUTHOR(S): T. W. Dombeck

SUBMITTED TO: Proceedings of the European Accelerator Conference, Rome, Italy, June 7-11, 1988

Los Alamos National Laboratory
Los Alamos, New Mexico 87545

To Be Submitted For Publication In The Proceedings Of The European Accelerator Conference, Rome, Italy, June 7-11, 1988.

PERFORMANCE OF THE LOS ALAMOS EXPANDING TELESCOPE*

T. Dombeck

On Behalf of the Los Alamos-Argonne Collaboration

Los Alamos National Laboratory, Los Alamos, NM 87545, USA.

ABSTRACT

An expanding telescope can produce a very low divergence particle beam, provided that the beam optics have sufficient quality in order not to introduce large aberrations. Even as late as two years ago there were no theoretical beamline codes, and little experimental work that could describe the third-order aberrations introduced by an expanding telescope. A project was undertaken at Los Alamos National Laboratory to perform these calculations, and to build a telescope to confirm the predictions. It was installed at Argonne National Laboratory during the summer of 1987 and tested in a 50 MeV H^- beam. The telescope consisted of a singlet eyepiece and triplet objective lens with a twenty times magnification. It performed to the design specifications of twenty-five micro-radians beam divergence with a parallel beam focus. The measured geometric aberrations were found to be in agreement with the computer calculations.

BEAMLINE, TELESCOPE, AND DIAGNOSTICS EQUIPMENT

The experiment was performed using the Argonne Laboratory 50 MeV H^- linear accelerator. The momentum spread of the beam incident into the telescope was measured to be less than 0.1%. The beam emittance was adjusted using collimators in the transport line between the accelerator and the telescope to yield the desired value near an rms of 0.06π-cm-mrad. With these settings we achieved a beam current near 250 microamps incident on the telescope at a 3 Hz pulse rate. Due to the low current densities, space-charge effects were negligible throughout the experiment.

The telescope is shown schematically in Fig. 1, and consisted of a singlet eyepiece and a triplet objective lens, each composed of permanent magnets. The overall length between the magnetic elements was 7.7 meters. The design magnification was twenty, providing a Gaussian-shaped spot with a 2.5-cm rms radius at the telescope exit. The beamline and telescope parameters are summarized in Table I.

The telescope diagnostics included a toroid, stripline beam position monitors, wire scanners, fluorescent screens, and wire harps. The positions of each of these devices is indicated in Fig. 1, and their sensitivities are summarized in Table I. These devices were used to align the beam and to obtain the correct tune to a level near 400 microradians in divergence. There was an intentional built-in redundancy in the diagnostics which proved valuable during the run.

BEAM CHARACTERIZATION EQUIPMENT

The telescope had a design specification of twenty-five microradians beam divergence with a parallel beam focus. Third-order geometric aberrations were predicted by computer calculations[1] to be a few micro-radian per cm^3, giving rise to angular deviations of up to 250 microradians at twice the rms beam radius. The characterization of the telescope optics at this precision required measurements in a range that had seldom, if ever, been achieved for a particle beam.

An optical method of imaging pinholes onto a fluor was developed to measure the beam quality out of the telescope. The equipment is shown schematically in Fig. 2, and was placed just downstream of the telescope objective lens. A plate with tiny pinholes was inserted into the expanded beam just downstream of the steering magnet in diagnostics box DB02. The incident H^- particles were stripped to H^+ everywhere in the plate except where the tiny pinholes intercepted the beam. The pinholes, having diameters of about 200 microns, were coated with a thin neutralizer foil, 8 micrograms/cm^2 in areal density, that converted half of the remaining H^- to neutral H^0. A large sweep magnet downstream of the pinhole plate removed all charged species leaving only the neutral H^0 beamlets to continue downstream. These penetrated a fluorescent screen placed at a distance of 10 meters. The pinholes were arranged in a rectilinear array on 1-cm centers, such that any distortion caused by the beam aberrations would appear as shifts in the centroids of the images from their expected positions. First-order shifts were a measure of the beam focus and steering, while third-order shifts were the result of spherical aberration. In propagating over the 10-m distance, the beamlets naturally grew in diameter, such that the observed pinhole widths also provided a measure of the local beam divergence.

Two cameras recorded the pinhole images in the detector chamber. One of these employed a cooled charged-coupled device (CCD) with a 27 micron pixel size on a grid of 512 rows by 512 columns. This camera viewed the entire beam spot (about a 10-cm diameter viewing area) with a magnification near 0.1. It was used to obtain information on beam focus and aberrations. The other camera was an 18-mm FPS videcon placed on the other side of the beamline. It was used at a magnification near unity, such that it imaged the width of individual pinholes to obtain a measure of the beam divergence. Either camera could be used by moving the appropriate mirror and fluor into place. This procedure did not require re-focus or re-calibration of the cameras. A calibration plate, inserted periodically at the fluor position, was used to check the geometric integrity of the CCD and videcon cameras.

A second optical method to characterize the beam used a precision grid of wires placed directly into the H^- beam in diagnostics box DB01 that cast shadows onto a fluor at a distance of 4.5 meters placed in DB02. The wire grid was stretched at 5-mm intervals and the wire positions were measured to a one micron precision. The 254 micron wide Ni wires used in the grid were the optimal thickness for the 4.5-m distance to the fluor in order to obtain a good beam divergence measurement. The shadow images were viewed on a RAREX fluor by a CCD camera (11.5-micron x 27-micron pixel size), placed at a 30° angle with respect to the beam axis. The camera pan, tilt and focus were adjusted remotely.

The parameters of the pinhole and wire shadow beam characterization equipment is summarized in Table II. A direct comparison was made between the wire shadow and the pinhole measurements to see if they gave the same results for beam divergence and aberrations.

DATA AND RESULTS

We tuned the telescope in steps during the run. In the first step, we adjusted quadrupole magnets in the transport line to achieve the desired spot size at the exit of the telescope and a roughly parallel beam focus. The spot size was measured using the wire harps, and we used wire shadows to achieve a beam focus parallel to within 100 microradians/cm by visual inspection of the average wire separation on the fluor image.

The final beam focus required small adjustments to the currents in three quadrupole trim coils wound around the beam pipe inside the permanent-magnets of the triplet objective lens. For this measurement we used a computer analysis of the pinhole image separations, where the first-order centroid shifts gave a measure of the telescope focus. Using this data, the trim-coil current settings to achieve a parallel beam were calculated using theoretical values of the R-matrix for the telescope elements. This required the solution of a set of simultaneous linear equations, and was accomplished in an iterative fashion, using the pinhole measurements and an on-line feedback program in an automatic closed-loop to adjust the trim coils. In this way we achieved a focus of ≤ 5 microradians/cm over the beam spot. In the final series of adjustments, the changes to the magnet field strengths amounted to only

0.1%. These values had to be calculated by computer, as it was virtually impossible to optimize these settings by manual adjustment.

With the telescope at its best tune, we measured the geometric aberrations. Fig. 3 shows one of the pinhole-pattern images taken during the run. The third-order aberration is evident in the barrel distortion, and the (X,Y) centroids were fit to obtain the aberration coefficients. Averaging over many such pictures, we obtained the third-order aberration coefficients given in Table III, along with their rms fluctuations determined from the data. These errors show that our camera system measured these coefficients to a precision from 2% to 10%. Also shown in Table III is the predictions of the various computer programs[2-4], and the agreement with the data is good.

From the pinhole width data we showed that the expanded beam had achieved the desired beam divergence of less than 25 microradians in both the x and y directions. The precision of this measurement was a fraction of a microradian. By adjusting the collimators in the transport line, we found that the divergence changed linearly with the input emittance into the telescope as expected for a constant spot size.

A direct comparison between the pinhole and the wire shadow measurements was made for a particular telescope setting. The aberration results are shown in Table IV. The third-order cubic terms in x and y determined from the wire shadows agreed within the errors with those determined from the pinholes. The third-order cross terms were consistent with zero from the wire shadow measurements, and were not in agreement with the pinhole data. We are currently investigating this discrepancy. A fit to the shadow profiles demonstrated the errorfunction shape that had been predicted[5], and the beam divergence obtained in this way agreed with the pinhole width data.

CONCLUSIONS

The important results from these measurements were: (a) a reliable measurement of the third-order aberrations of the telescope that agreed with the computer calculations, (b) a confirmation that the beam divergence was emittance dominated and scaled linearly with the collimator settings in the transport line, (c) a demonstration that the pinhole data could be employed successfully in an automatic beam tuning process, and (d) a demonstration that wire shadows give similar results in beam characterization as the pinhole method, though more work is needed to understand the discrepancies.

The next major initiative for the telescope at Argonne is an upgrade using a large bore (1.5 m) electro-magnet in place of the existing (0.3 m) objective lens. Octupole correcting coils will be installed to remove the third-order aberration distortion. This experiment will be run in the late summer of 1988.

TABLE I. BEAMLINE AND TELESCOPE PARAMETERS

Beam	50 MeV H^-
Momentum spread	< 0.1%
Emittance	0.06π-cm-mrad (rms)
Telescope length	7.7 m
Eyepiece	quadrupole singlet (permanent magnet)
Objective lens	quadrupole triplet (permanent magnets)
Objective lens aperture	0.3 m
Telescope magnification	20 x
Spot size	2.5-cm radius (rms)
Beam divergence	< 25 microrad (rms)
Stripline beam position monitor resolution	±45 microns
Wire scanners:	
wire size	50-micron diameter (Ni)
position resolution	±20 microns
Wire harps:	
wire spacing	30 wires spaced 5 mm apart
wire size	500 microns wide by 12 microns thick (Ni)

TABLE II. CHARACTERIZATION EQUIPMENT

Pinhole diagnostic:	
pinhole widths	200 microns
pinhole array	12-cm x 12-cm array on 1-cm centers
distance from pinholes to fluor	10 m
CCD camera	512 x 512 array of 27 micron pixels, magnification = 0.1
FPS videcon camera	18 mm x 18 mm active area, with 30 micron pixels, magnification = 1.0
Wire shadow diagnostic:	
wire grid	20-cm x 20-cm array on 5-mm centers
wire size	254 micron diameter (Ni)
wire spacing tolerance	measured to 1 micron
distance from grid to fluor	4.5 m
CCD camera	11.5-micron x 27-micron pixels, viewing fluor at 30°, magnification near 0.1 (adjustable)

TABLE III. ABERRATION RESULTS FROM THE PINHOLE MEASUREMENTS

Coefficient	Measurement*	MARYLIE[2]	GIOS[3]	MOTR[4]
θ/X^3	-0.59 ± 0.06	-0.47	-0.51	-0.54
θ/XY^2	-2.16 ± 0.04	-2.28	-2.38	-2.34
ϕ/Y^3	-1.33 ± 0.02	-1.36	-1.39	-1.23
ϕ/YX^2	-1.97 ± 0.04	-2.28	-2.39	-2.31

*Units are microradians/cm^3.

TABLE IV. ABERRATION MEASUREMENT COMPARISON BETWEEN PINHOLES AND WIRE SHADOWS

Coefficient	Pinholes*	Wire Shadows*
θ/X^3	-0.74 ± 0.06	-0.78 ± 0.04
ϕ/Y^3	-1.27 ± 0.02	-1.18 ± 0.05

*Units are microradians/cm^3.

REFERENCES

* Work performed under the auspices of the U. S. Department of Energy and supported by the U. S. Army Strategic Defense Command.

[1]L. Schweitzer, C. T. Mottershead, and E. Heighway, "The Functional Dependence of Particle Divergence (X',Y') on Position (X,Y) at the Output of an Expansion Telescope as Simulated by the Third Order Code MARYLIE," Los Alamos National Laboratory Technical Note AT-3:87-22 (July, 1987).

[2]A. Dragt, The MARYLIE Program, University of Maryland.

[3]H. Wollnik, The GIOS Program, University of Giessen.

[4]A. Thiessen, The MOTER Program, Los Alamos National Laboratory.

[5]J. McHead, "[illegible] with Particle Beams," AFWL/AWY unpublished report (March, 1986).

FIGURE CAPTIONS

Fig. 1. The expanding telescope for the 50 MeV H^- beam is shown schematically. The eyepiece and objective lens were composed of permanent magnets. The positions of the telescope diagnostics are also indicated. The parameters of the telescope elements are summarized in Table I.

Fig. 2. The beam elements just downstream of the objective lens to the beam stop that were used for beam characterization are shown schematically. The significant parts of the line are numbered and identified in the figure, while their operation is discussed in the text.

Fig. 3. A data picture taken during the run is presented showing the pinhole centroid images. The "barrel distortion" characteristic of the third-order geometric aberrations is evident. The two extra holes in the middle of the picture are markers to indicate the center of the pinhole plate.

Fig. 4. A data picture taken during the run of the wire shadow images is shown. The same "barrel distortion" evident in Fig. 3 is also seen here.

LOS ALAMOS NPB/GTA TELESCOPE AT ANL

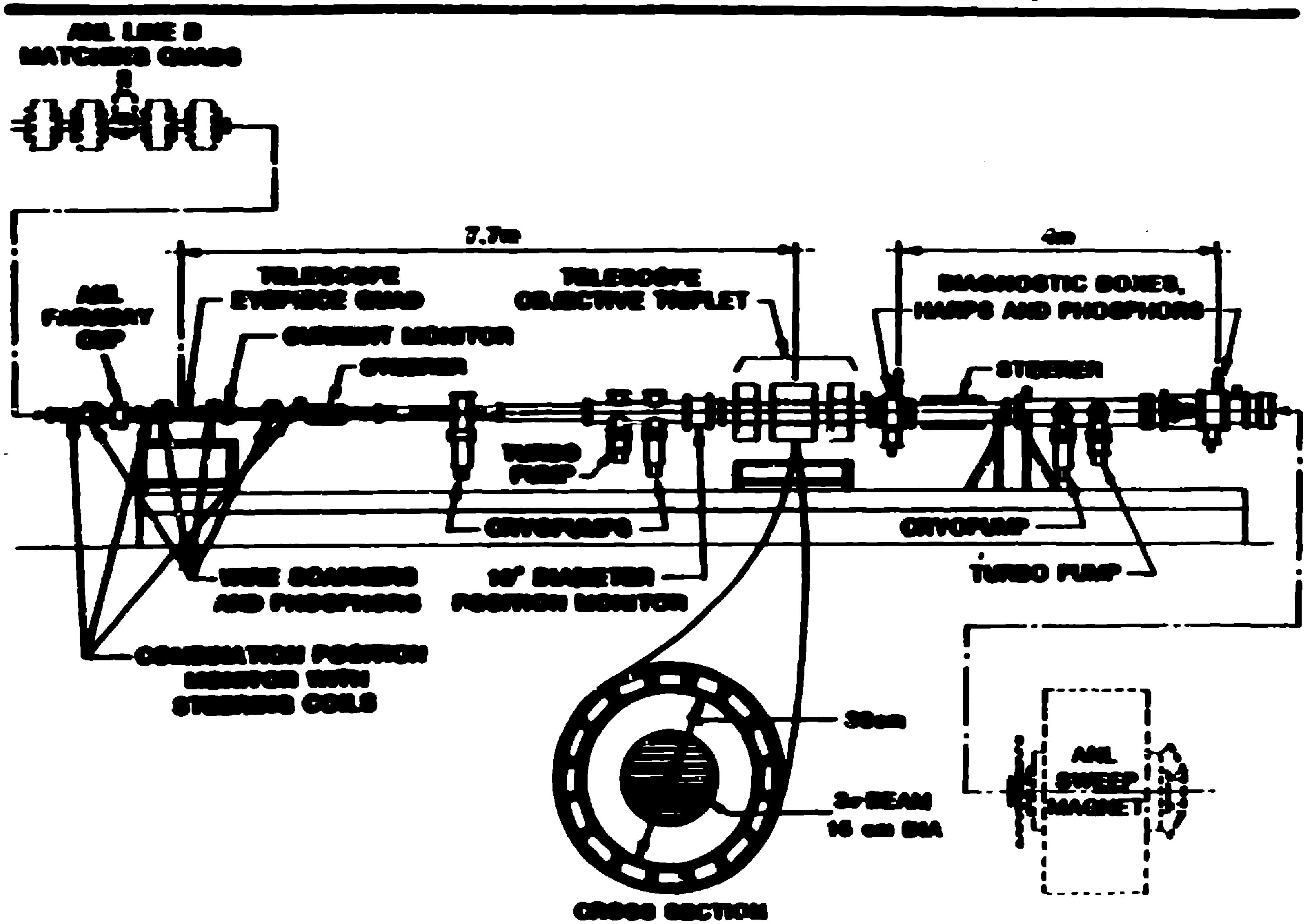

Fig. 1

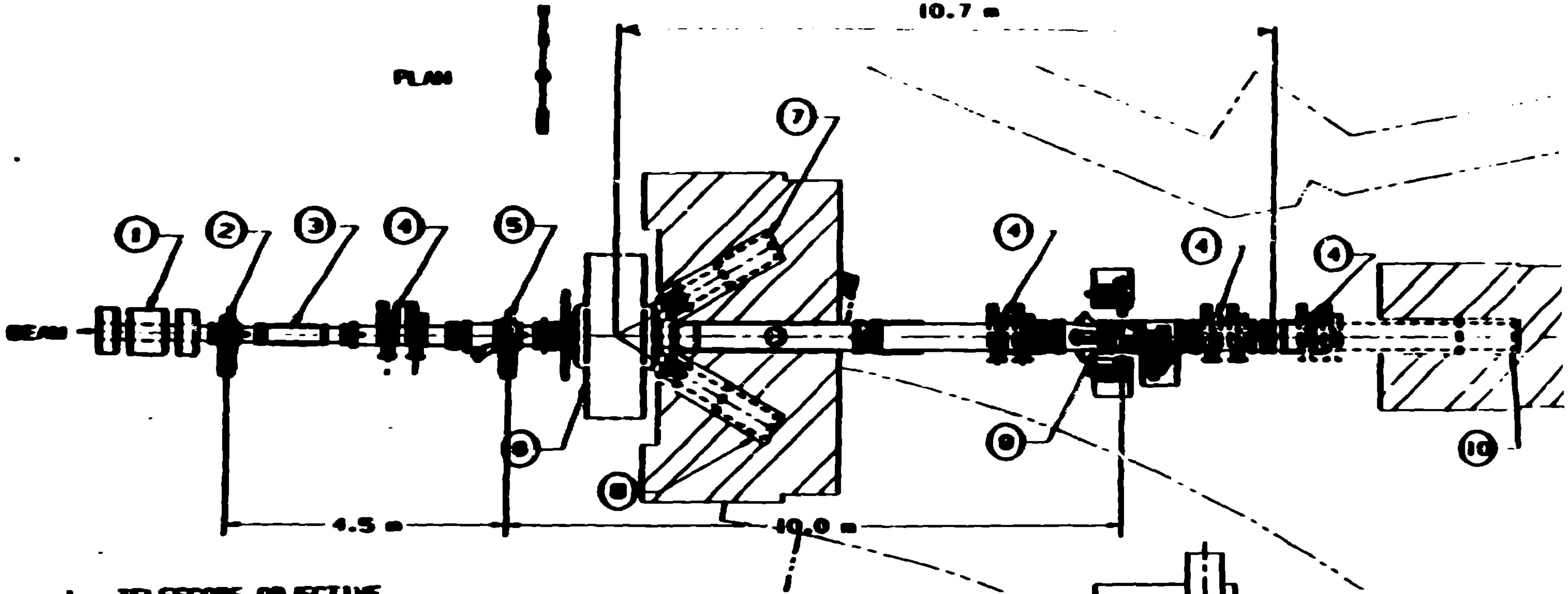

1 TELESCOPE OBJECTIVE
2 OBD1
3 HMD3
4 VACUUM PUMPS
5 OBD2 PINHOLE FOIL
6 SWEEP MAGNET
7 H^- BEAM STOP
8 H^0 BEAM STOP
9 DETECTOR CHAMBER
10 BEAM STOP
11 MIRROR
12 FLUOR
13 CCD IMAGER
14 FPS VIDICON
15 VACUUM IMAGER

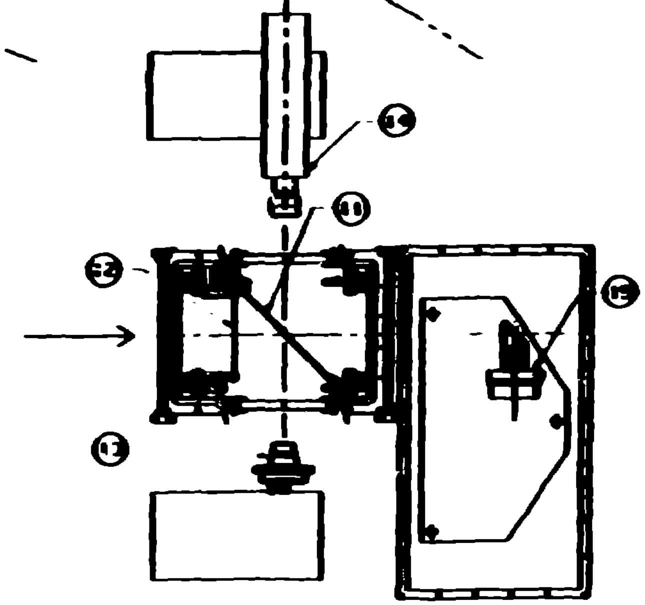

9 DETECTOR CHAMBER

Fig 2

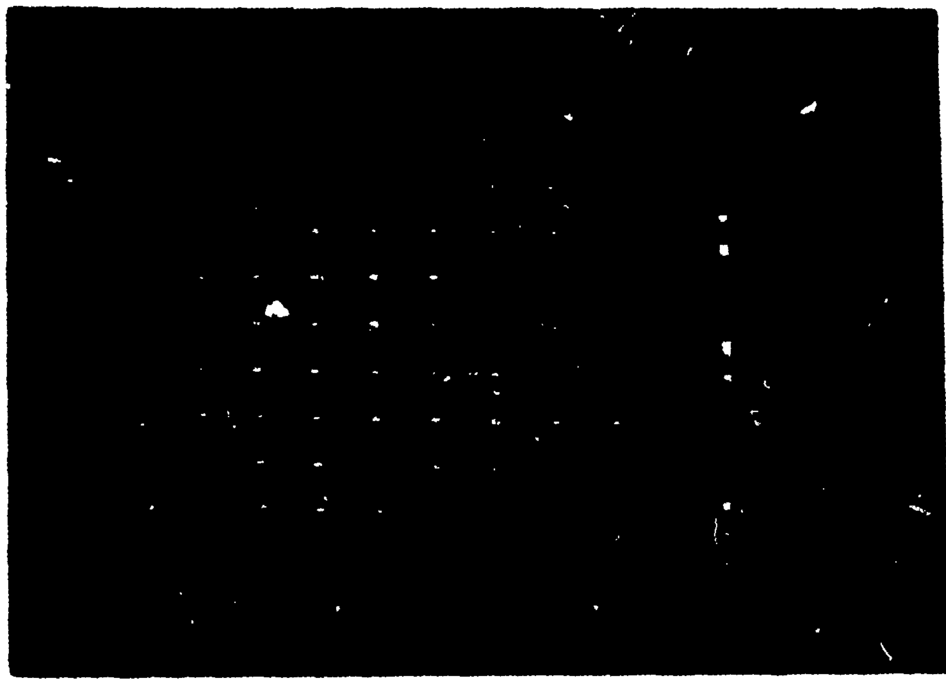

Fig. 3.

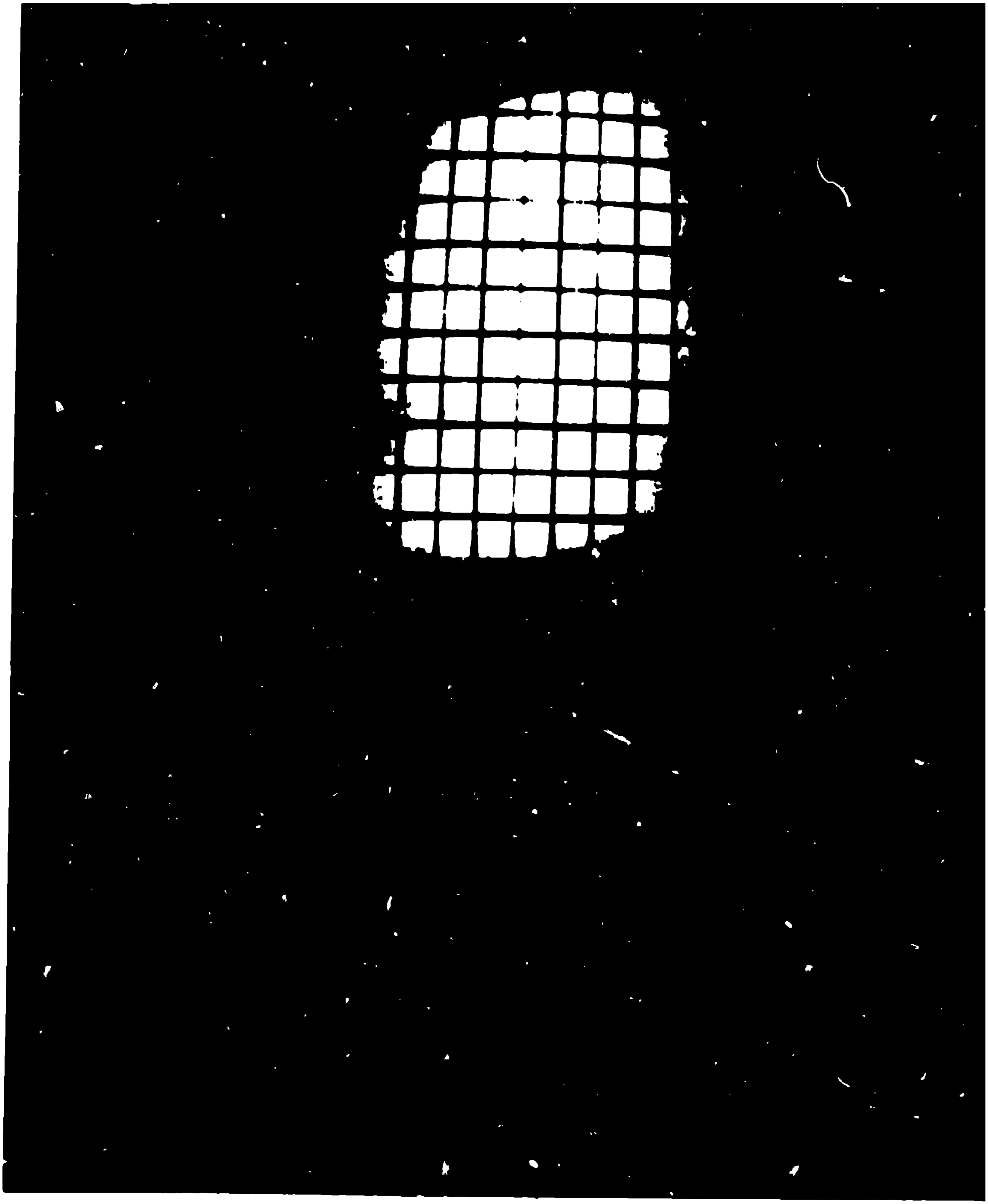

Fig. 4